

Search for methylamine in high mass hot cores[★]

N. F. W. Ligterink^{1,2}, E. D. Tenenbaum¹, and E. F. van Dishoeck^{1,3}

¹ Leiden Observatory, Leiden University, PO Box 9513, 2300 RA Leiden, The Netherlands
e-mail: ligterink@strw.leidenuniv.nl

² Raymond and Beverly Sackler Laboratory for Astrophysics, Leiden Observatory, Leiden University, PO Box 9513, 2300 RA Leiden, The Netherlands

³ Max-Planck Institut für Extraterrestrische Physik (MPE), Giessenbackstr. 1, 85748 Garching, Germany

Received 21 August 2014 / Accepted 18 December 2014

ABSTRACT

Aims. We aim to detect methylamine, CH₃NH₂, in a variety of hot cores and use it as a test for the importance of photon-induced chemistry in ice mantles and mobility of radicals. Specifically, CH₃NH₂ cannot be formed from atom addition to CO whereas other NH₂-containing molecules such as formamide, NH₂CHO, can.

Methods. Submillimeter spectra of several massive hot core regions were taken with the *James Clerk Maxwell* Telescope (JCMT). Abundances are determined with the rotational diagram method where possible.

Results. Methylamine is not detected, giving upper limit column densities between 1.9–6.4 × 10¹⁶ cm⁻² for source sizes corresponding to the 100 K envelope radius. Combined with previously obtained JCMT data analysed in the same way, abundance ratios of CH₃NH₂, NH₂CHO and CH₃CN with respect to each other and to CH₃OH are determined. These ratios are compared with Sagittarius B2 observations, where all species are detected, and to hot core models.

Conclusions. The observed ratios suggest that both methylamine and formamide are overproduced by up to an order of magnitude in hot core models. Acetonitrile is however underproduced. The proposed chemical schemes leading to these molecules are discussed and reactions that need further laboratory studies are identified. The upper limits obtained in this paper can be used to guide future observations, especially with ALMA.

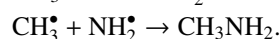
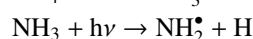
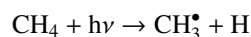
Key words. astrochemistry – line: identification – methods: observational – stars: formation – ISM: abundances – ISM: molecules

1. Introduction

Complex organic molecules are thought to be formed primarily on dust grains in dense cores, see reviews by [Herbst & van Dishoeck \(2009\)](#) and [Caselli & Ceccarelli \(2012\)](#). Before the onset of star formation, the atomic and molecular reservoir is contained in large dark clouds. Due to the high densities (≥10⁴ cm⁻³) and low temperatures (10 K) reached in these environments, gas-phase species will freeze out on sub-micron sized grains forming ice mantles on timescales shorter than the lifetime of the cloud. It is here that atoms and molecules can potentially react with each other to form the zeroth order ice species like ammonia, methane, water and methanol. UV radiation interacts with these ice mantles by dissociating molecules to produce radicals and by photodesorbing species back to the gas phase. If these radicals are sufficiently mobile, they can find each other on the grain and react to form even more complex first generation (organic) species ([Garrod & Herbst 2006](#)). However, it is not entirely clear if UV radiation is essential to form these complex molecules or whether they can also be formed just by thermal processing and atom bombardment of solid CO with C, N and O atoms ([Tielens & Charnley 1997](#)).

In this context methylamine, CH₃NH₂, is a particularly interesting molecule, since its formation is hypothesised by [Garrod et al. \(2008\)](#) to be completely dependent on radicals produced

by UV photons, and is one of the few molecules that can definitely not be produced in the routes starting from solid CO:



These radicals can form in the ice mantles in the dark cloud or in the protostellar phase through cosmic-ray induced photons and/or UV photons from the protostar. After gravitational collapse of the cloud and formation of a protostar, the dust around it will start to warm up. The increased temperature will cause the radicals to become mobile on the grains and react with each other, forming methylamine. Further heating will evaporate the formed methylamine from the grain and raise its gas-phase abundance.

Another interesting amine-containing molecule is formamide, NH₂CHO. This is so far the most abundantly observed amine-containing molecule (e.g., [Halfen et al. 2011](#); [Bisschop et al. 2007](#)), making it an interesting molecule to compare with other amines like methylamine. In contrast with CH₃NH₂, this molecule can possibly be produced by reactions of H and N with solid CO. The comparison of the abundances of these two species could potentially give more information about the relative importance of UV-induced versus thermal grain surface reactions.

Hot cores are particularly well-suited to study methylamine. These high mass star-forming regions reach high temperatures

[★] Appendices are available in electronic form at <http://www.aanda.org>

Table 1. Source list and source parameters.

Source	RA J2000	Dec J2000	θ_S^a AU	θ_B^a AU	L^a L_\odot	d^a (kpc)	V_{LSR} (km s ⁻¹)	ΔV (km s ⁻¹)	$\delta\nu$ (km s ⁻¹)	rms (mK)
AFGL 2591	20:29:24.60	+40:11:18.9	1800	21 000	2.0E+05	3.3	-5.5	4.0	1.28	10
G24.78	18:36:12.60	-07:12:11.0	13 000	162 000	7.9E+05	7.7	111.0	6.3	1.28	9
G31.41+0.31	18:47:34.33	-01:12:46.5	7840	166 000	2.6E+05	7.9	98.7	7.3	1.28	7
G75.78	20:21:44.10	+37:26:40.0	5600	86 100	1.9E+05	4.1	-0.04	5.6	1.28	9
IRAS 18089-1732	18:11:51.40	-17:31:28.5	2750	49 000	3.2E+04	2.3	33.8	4.5	1.28	9
IRAS 20126+4104	20:14:26.40	+41:13:32.5	1753	34 400	1.3E+04	1.6	-3.8	6.0	1.28	10
NGC 7538 IRS1	23:13:45.40	+61:28:12.0	4900	58 800	1.3E+05	2.8	-57.4	4.0	1.28	10
W3(H ₂ O)	02:27:04.60	+61:52:26.0	2400	42 000	2.0E+04	2.0	-46.4	5.0	1.28	11
W 33A	18:14:38.90	-17:52:04.0	4500	84 000	1.0E+05	4.0	37.5	4.9	1.28	11

Notes. ^(a) Data for AFGL 2591 taken from Rygl et al. (2012). Other data taken from Bisschop et al. (2007) and Isokoski et al. (2013).

between 100 to 300 K and are known for their rich complex organic chemistry (Walmsley 1992; van Dishoeck & Blake 1998; Tielens & Charnley 1997; Ehrenfreund & Charnley 2000; Caselli & Ceccarelli 2012). The ice covered grains move inwards to the protostar and will heat up. When sufficient temperatures are reached, molecules will start to desorb depending on their respective binding energies. Less abundant molecules mixed with water ice will desorb together with water around 100 K.

Previous detections of methylamine have all been made toward the galactic center. Kaifu et al. (1974) first detected CH₃NH₂ in Sagittarius B2 and Orion A. Later that same year Fourikis et al. (1974) reported the detection of methylamine in the same sources, but with a different telescope. Much more sensitive surveys by Turner (1991), Nummelin et al. (2000), Halfen et al. (2013), Belloche et al. (2013) and Neill et al. (2014) also all detected methylamine lines toward Sgr B2, with typical inferred abundance ratios with respect to NH₂CHO between 0.5 to 3. No detections of methylamine have been reported in sensitive surveys with modern detectors toward Orion, however (Blake et al. 1987; Turner 1991; Sutton et al. 1995; Schilke et al. 1997; Crockett et al. 2014).

To study the importance of UV processing of ice-covered dust grains, we present the results of searches for methylamine in a number of hot cores (see Table 1). These results are combined and compared with data from Bisschop et al. (2007) and Isokoski et al. (2013), which were taken toward the same hot cores with the same telescope and analysis method and include detections of NH₂CHO and other nitrogen-containing species. In Sect. 2 the observational details are given, followed by the analysis method in Sect. 3. Section 4 summarizes all the results of our analysis and these are discussed in Sect. 5. Finally conclusions are drawn in Sect. 6.

2. Observations

Observations were performed with the *James Clerk Maxwell* Telescope (JCMT)¹ on the sources listed in Table 1 between July 2010 and August 2011. The sources were selected based on their particularly rich chemistry, being isolated, having narrow line widths to prevent line confusion and on their relatively nearby distance (Bisschop et al. 2007; Fontani et al. 2007; Rathborne et al. 2008; Isokoski et al. 2013).

¹ The *James Clerk Maxwell* Telescope is operated by the Joint Astronomy Centre on behalf of the Science and Technology Facilities Council of the United Kingdom, the National Research Council of Canada, and (until 31 March 2013) the Netherlands Organisation for Scientific Research.

Table 2. Methylamine transitions observed in this study.

Transition	Freq. (MHz)	E_{up} (K)	A (s ⁻¹)	g_{up}
4 ₂ → 4 ₁ ^a	229 310.298	36.9	1.32E-05	108
7 ₂ → 7 ₁ ^a	229 452.603	75.5	5.88E-06	60
8 ₂ → 8 ₁ ^b	235 735.037	92.8	6.13E-05	204
6 ₂ → 6 ₁ ^a	236 408.788	60.8	5.94E-05	52
2 ₂ → 2 ₁ ^a	237 143.530	22.0	3.82E-05	60
10 ₂ → 10 ₁ ^c	260 293.536	132.7	2.26E-05	52

Notes. Data from JPL database for molecular spectroscopy. ^(a) Transition observed in all sources. ^(b) Only observed in W3(H₂O). ^(c) Only observed in W3(H₂O) and NGC 7538 IRS1.

Nummelin et al. (1998) detected methylamine emission lines between 218 to 263 GHz toward Sgr B2N. Therefore the RxA3 front-end double side band receiver, functioning between 210 to 276 GHz, was chosen to observe the hot cores. The 250 and 1000 MHz wide back-end ACSIS configurations were used. A number of methylamine transitions covering a range of excitation energies were selected in this frequency range based on high Einstein A coefficients and lack of line confusion (Table 2). However, not all transitions were observed for all sources. The 235 735 MHz transition was only recorded for W3(H₂O) and the 260 293 MHz transition only toward W3(H₂O) and NGC 7538 IRS1.

Because double side band spectra were obtained, our spectra contain transitions from two different frequency regimes superposed. To disentangle lines from the two side bands, each source was observed twice with an 8 MHz shift in the local oscillator setting between the two observations. This allows each transition to be uniquely assigned to either of the two side bands.

In the 230 GHz band, the JCMT has a beam size (θ_B) of 20–21''. Spectra were scaled from the antenna temperature scale, T_A^* , to main beam temperature, T_{MB} , by using the main beam efficiency of 0.69 at 230 GHz. Integration times were such that T_{rms} is generally better than 10 mK for data binned to 1.3 km s⁻¹ velocity bins. Noise levels were improved by adding the shifted spectra together in a narrow frequency region around the CH₃NH₂ lines, effectively doubling the integration time.

3. Data analysis

To analyse the data, exactly the same method as described by Bisschop et al. (2007) and Isokoski et al. (2013) was used.

It will be shortly reiterated here. The hot core spectra corrected for source velocity were analysed with the “Weeds” extension (Maret et al. 2011) of the Continuum and Line Analysis Single-dish Software (CLASS²) coupled with the Jet Propulsion Laboratory (JPL³) database for molecular spectroscopy (Pickett et al. 1998). Focus was on identifying the transitions of methylamine listed in Table 2, but other lines in the spectra were measured as well (see Table A.1). After each positive identification the integrated main-beam temperature, $\int T_{\text{MB}} dV$, was determined by Gaussian fitting of the line. From the integrated main-beam intensity the column density N_{up} and thus the beam-averaged total column density N_{T} could be determined, assuming Local Thermodynamic Equilibrium (LTE) at a single excitation temperature T_{rot} :

$$\frac{3k \int T_{\text{MB}} dV}{8\pi^3 \nu \mu^2 S} = \frac{N_{\text{up}}}{g_{\text{up}}} = \frac{N_{\text{T}}}{Q(T_{\text{rot}})} e^{-E_{\text{up}}/T_{\text{rot}}} \quad (1)$$

where g_{up} is the level degeneracy, k the Boltzmann constant, ν the transition frequency, μ the dipole moment and S the line strength. $Q(T_{\text{rot}})$ is the rotational partition function and E_{up} is the upper state energy in Kelvin.

In case of a non-detection, 3σ upper limits were determined from the root mean square (rms) of the base line of the spectra in combination with the velocity resolution δv and line width ΔV :

$$\sigma = 1.2 \sqrt{\delta v \Delta V} \cdot \text{rms} \quad (2)$$

ΔV is estimated from other transitions (see Table 1) in the spectra, for example from the nearby $\text{H}_2\text{CS } 7_1 \rightarrow 6_1$ transition, and assumed to be the same for all transitions in the spectral range. A telescope flux calibration error of 20% is taken into account in the 1.2 factor. The 3σ value is then used in the same way as the main-beam intensity of detected lines to obtain the upper limit on the total column density through Eq. (1).

Since no rotational temperature can be determined for a non-detection, this has to be estimated. In the models of Garrod et al. (2008) the peak abundance temperatures for methylamine range from 117 to 124 K depending on the model used. Öberg (2009) determined that methylamine forms in CH_4/NH_3 UV irradiation experiments and sublimates at 120 K. There is a small difference between laboratory and hot core desorption temperatures, because of the pressure difference between the two. Also, if CH_3NH_2 is embedded in water ice the desorption temperature will probably be limited to roughly 100 K, when water desorbs in space. Therefore T_{rot} is assumed to be 120 K when methylamine lines could not be identified, but the effects of lower and higher rotation temperatures are explored as well.

Correction for beam dilution is done in the same way as Bisschop et al. (2007):

$$\eta_{\text{BF}} = \frac{\theta_{\text{S}}^2}{\theta_{\text{S}}^2 + \theta_{\text{B}}^2} \quad (3)$$

resulting in the source-averaged column density:

$$N_{\text{S}} = \frac{N_{\text{T}}}{\eta_{\text{BF}}} \quad (4)$$

The beam diameter θ_{B} is set at 21". For the source diameter, θ_{S} , values have been taken from Bisschop et al. (2007) and Isokoski et al. (2013) and constitute the area where the temperature is

100 K or higher and hot gas-phase molecules are present. Both beam and source diameters are listed in AU in Table 1. Using the CASSIS line analysis software⁴ it was verified that the source-averaged column densities are still small enough that the observed lines are optically thin.

4. Results and comparison with astrochemical models

4.1. CH_3NH_2 limits

Figure 1 presents examples of spectra obtained for our sources, whereas Fig. A.2 shows the 2_2-2_1 line in all sources. In general, no transitions of CH_3NH_2 are detected. Only one possible methylamine transition is identified in G31.41+0.31 coincident with the $6_2 \rightarrow 6_1$ line at 236 408 MHz, with an integrated intensity of 0.44 K km s^{-1} . Following the procedure summarized in Sect. 3, a column density of $3.4 \times 10^{17} \text{ cm}^{-2}$ is inferred from this line assuming $T_{\text{rot}} = 120 \text{ K}$. However, modelling of the spectrum shows that the other targeted CH_3NH_2 lines, $4_2 \rightarrow 4_1$ and $2_2 \rightarrow 2_1$, should have comparable or even higher intensities if this identification is correct (Fig. A.1). The $8_2 \rightarrow 8_1$ line should be readily detected but was not observed toward G31.41+0.31. This makes it unlikely that the detected feature belongs to methylamine, since we would expect to see at least two other CH_3NH_2 transitions in our spectrum.

In Fig. 2 upper limit column densities of the six investigated transitions of methylamine are plotted versus rotational temperature taking a typical $3\sigma = 0.100 \text{ K km s}^{-1}$. At 120 K the $8_2 \rightarrow 8_1$, 235 735 MHz transition gives the lowest limits on the column densities, see Fig. 2. However, since this particular transition was only included in the observations for one source, the second most sensitive transition at 120 K, $2_2 \rightarrow 2_1$, will be used (see Fig. A.2 for a blow-up of this particular spectral region in all investigated sources). All following molecular ratios are based on CH_3NH_2 column densities obtained from this line, assuming $T_{\text{rot}} = 120 \text{ K}$. The corresponding upper limits are presented in Table 3.

4.2. Abundance ratio comparison

Combined with NH_2CHO and CH_3OH column densities from Bisschop et al. (2007) and Isokoski et al. (2013) derived in the same way, abundance ratios for methylamine and formamide with respect to each other and to methanol are calculated. These ratios are listed in Table 3. Methanol is chosen as a reference since it is the most readily observed complex organic molecule. Its disadvantage is that some of the transitions have high optical depth and that a cold component may be present (Isokoski et al. 2013), but this is circumvented by only taking the warm methanol column density derived from optically thin lines. Abundances relative to methanol rather than H_2 are preferred since the H_2 column depends on extrapolation of dust models to smaller scales than actually observed (Bisschop et al. 2007). Another point that needs to be taken into account is that the models of Garrod et al. (2008) do show a slight overproduction of CH_3OH , which could influence the comparison between the ratios. Overall, the abundance ratios are estimated to be accurate to a factor of a few.

It should be noted that methylamine and formamide have significantly different dipole moments (1.31 and 3.73 Debye respectively) and could therefore be excited in different ways.

² <http://www.iram.fr/IRAMFR/GILDAS>

³ <http://spec.jpl.nasa.gov>

⁴ CASSIS has been developed by IRAP-UPS/CNRS (<http://cassis.irap.omp.eu>).

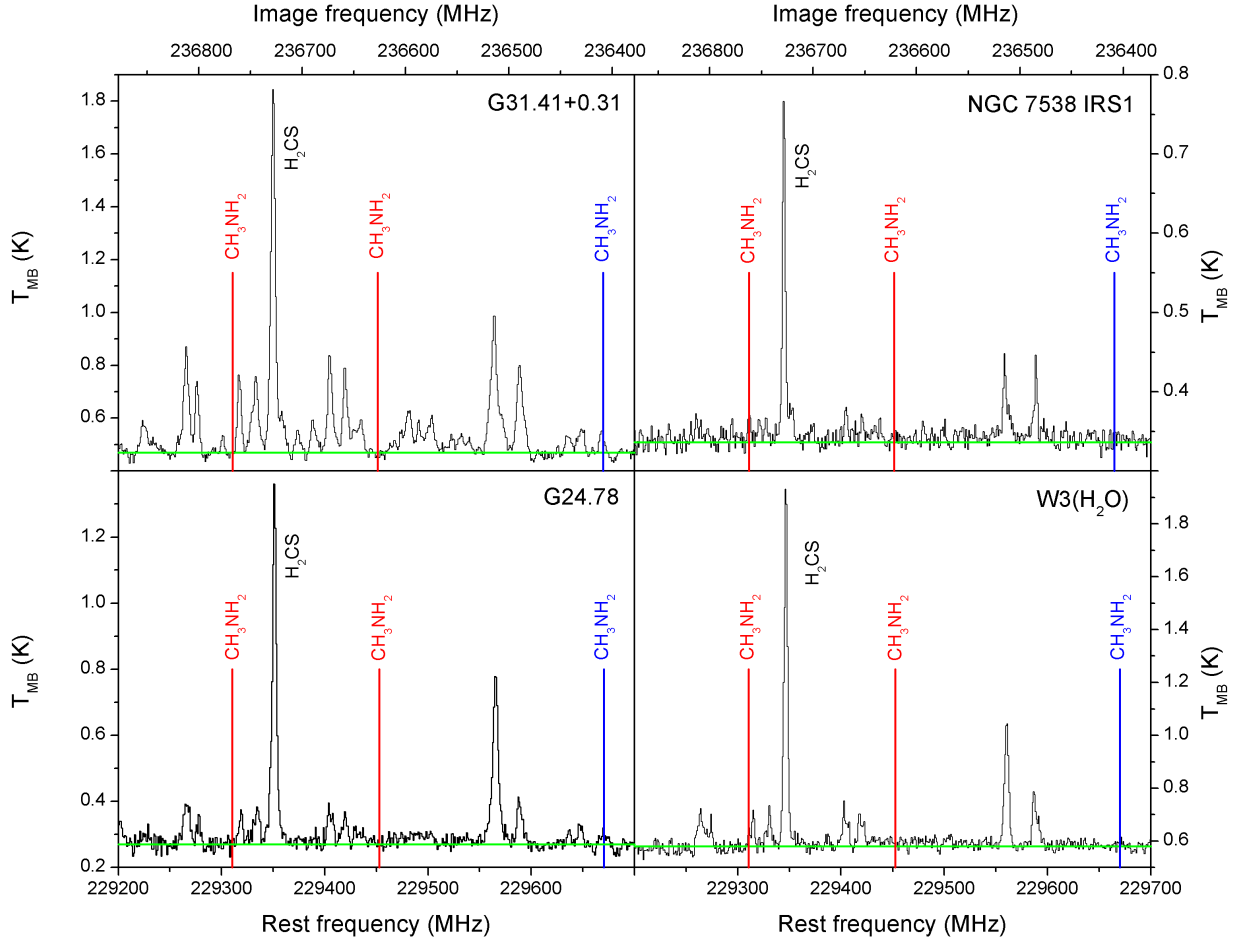


Fig. 1. JCMT spectra of the massive hot cores G31.41+0.31, G24.75, NGC 7538 IRS1 and W3(H₂O). The 229 310 and 229 452 MHz transitions in the lower sideband are indicated in red and that at 236 408 MHz in the upper sideband in blue. In green is the baseline, obtained by fitting line free portions of the spectrum. In all spectra the H₂CS 7₁ → 6₁ transition at 236 726 MHz is fitted to determine the typical linewidth in the sources, as listed in Table 1.

Formamide has a larger critical density than methylamine, so the situation could arise where the critical density is not reached for formamide or even both molecules. The corresponding excitation temperatures will then be lower. In particular, the situation in which the critical density is not reached for formamide but is for methylamine, could affect the inferred ratios. As can be seen from Fig. 2, if T_{rot} drops from 120 to 50 K, the column density drops by a factor of a few, depending on transition. If T_{rot} were 120 K for methylamine but 50 K for formamide, the observed column density of formamide would be lower than that listed here and thus result in a higher CH₃NH₂/NH₂CHO ratio. We note, however, that there is no observational evidence that T_{rot} is systematically lower than 100 K for formamide (Bisschop et al. 2007).

Table 3 includes the observational results toward Sgr B2, the only source where methylamine is firmly detected, from Turner (1991), Belloche et al. (2013) and Neill et al. (2014). These results, obtained over the course of more than two decades, agree well with each other within the estimated uncertainties due to slightly different adopted source sizes. Nummelin et al. (2000) also detect methylamine in their Sgr B2 survey but find a surprisingly small beam filling factor and consequently very large column density compared with most other complex organic molecules. If their beam filling factor for CH₃NH₂ is taken to be the same as for NH₂CHO, the Nummelin et al. (2000) ratios are more in line with those derived by Turner (1991),

Belloche et al. (2013) and Neill et al. (2014). The non-detections of methylamine toward the chemically rich and well studied Orion hot core imply abundance limits that are at least a factor of 5 lower than for Sgr B2 (Neill et al. 2014; Crockett et al. 2014).

Table 3 also contains the model results from Garrod et al. (2008), who present three hot core models which differ from each other by their warm-up timescale from 10 to 200 K. The timescales for F(ast), M(edium) and S(low) are 5×10^4 , 2×10^5 and 1×10^6 years, respectively, and start after the cold collapse phase. In the slow models more time is spent in the warm-up phase where radicals are mobile. Values used in this comparison are taken from the so-called reduced ice composition, where cold phase methane and methanol abundances were modified to match observations of these ices toward W33A, NGC 7538 IRS9 and Sgr A*, see Gibb et al. (2000). Another comparison can be made with the gas-phase abundances in protoplanetary disk models of Walsh et al. (2014) which have similar or higher densities and temperatures as in protostellar cores. Their ratios range from 7.2×10^{-1} to 6.5×10^{-2} for CH₃NH₂/CH₃OH, 4.2×10^{-1} to 1.5 for CH₃NH₂/NH₂CHO and 1.7 to 8.8×10^{-2} for the NH₂CHO/CH₃OH. These ratios are close to the predicted values of Garrod et al. (2008) listed in Table 3, which may be partly due to using the same surface-chemistry network.

From Table 3 several trends become apparent for our results. The CH₃NH₂/NH₂CHO limits lie about an order of magnitude

Table 3. Upper limit column densities and abundance ratios for methylamine.

Source	N_{S,CH_3NH_2} cm^{-2}	CH_3NH_2/NH_2CHO	CH_3NH_2/CH_3OH	NH_2CHO/CH_3OH	NH_2CHO_{upper}/CH_3OH
Model F		1.1	3.4E-02	3.1E-02	3.1E-02
Model M		1.7	1.0E-01	7.3E-02	7.3E-02
Model S		1.3	1.3E-01	1.0E-01	1.0E-01
AFGL 2591	<1.9E+16	–	–	<3.9E-01	–
G24.78	<2.4E+16	<3.3E+01	<8.5E-02	2.6E-03	9.0E-04
G31.41+0.31	<5.8E+16	<2.8E+01	<4.9E-02	1.8E-03	3.8E-03
G75.78	<3.5E+16	<1.7E+02	<3.1E-01	1.8E-03	2.6E-02
IRAS 18089-1732	<4.2E+16	<5.0E+01	<1.9E-01	3.8E-03	7.9E-03
IRAS 20126+4104	<6.4E+16	–	<2.2	–	–
NGC 7538 IRS1	<2.0E+16	<3.5E+01	<1.8E-01	4.8E-03	2.1E-04
W3(H ₂ O)	<5.0E+16	<3.9E+01	<5.0E-02	1.3E-03	6.4E-04
W3(H ₂ O)*	<1.7E+16	<1.3E+01	<1.7E-02	1.3E-03	6.4E-04
W 33A	<5.7E+16	<2.7E+01	<2.9E-01	1.1E-02	4.6E-03
Sgr B2 ^a	1.2E+14	5.7E-01	1.7E-02	1.3E-02	
Sgr B2(M) ^b	4.5E+16	3.2	1.7E-02	5.2E-03	
Sgr B2(N) ^b	6.0E+17	4.3E-01	3.3E-02	7.8E-02	
Sgr B2(N) ^c	5.0E+17	2.1	1.0E-01	4.8E-02	
Orion Compact Ridge ^d	–	–	–	1.6E-03	

Notes. Column densities for the assumed source size and upper limit abundance ratios for methylamine, derived from the 2_2-2_1 line assuming $T_{rot} = 120$ K. The values for NH_2CHO and CH_3OH were taken from [Bisschop et al. \(2007\)](#) and [Isokoski et al. \(2013\)](#). The upper limits of NH_2CHO were determined by our own re-analysis of the [Bisschop et al. \(2007\)](#) data and taken from the appendix of [Isokoski et al. \(2013\)](#). ^(*) Column density calculated for the 8_2-8_1 line.

References. ^(a) [Turner \(1991\)](#), beam sizes between 65'' and 107'', assuming no beam dilution; ^(b) [Belloche et al. \(2013\)](#), beam sizes between 25'' and 30'', assuming a 3'' source size for (N) and 5'' source size for (M); ^(c) [Neill et al. \(2014\)](#), beam sizes between 10'' and 40'', assuming source size of 2.5''; and ^(d) [Crockett et al. \(2014\)](#) beam sizes between 44'' and 11'' and assuming a 10'' size of the Compact Ridge.

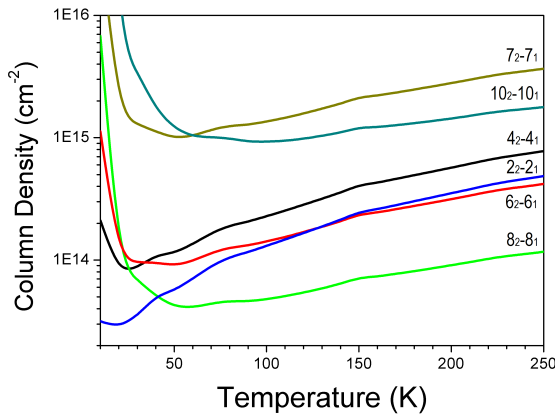


Fig. 2. Column densities for the six methylamine transitions plotted versus temperature. This plot is made for a 3σ limit of 0.1 K km s⁻¹, as found for W3(H₂O). This figure demonstrates that the 8_2-8_1 transition (green) gives the most sensitive limits on column density for the relevant range of excitation temperatures in hot cores, when observed. The other five transitions ($4_2 \rightarrow 4_1$, black; $7_2 \rightarrow 7_1$, gold; $10_2 \rightarrow 10_1$, cyan; $2_2 \rightarrow 2_1$, blue and $6_2 \rightarrow 6_1$, red) clearly imply higher column densities. Only below 40 K does the $2_2 \rightarrow 2_1$ line give lower column density limits.

above model values whereas the CH_3NH_2/CH_3OH limit approximately matches with theoretical predictions. Because the observed values are actually 3σ upper limits, this suggests that models overproduce CH_3NH_2 . For the sources with the most stringent limits, such as G31.41+0.31 and the 8_2-8_1 line in W3(H₂O), the CH_3NH_2/CH_3OH limits are comparable or even lower than the abundance ratios for Sgr B2. The third ratio, NH_2CHO/CH_3OH , is also found to be lower than the models by up to one order of magnitude.

Close inspection of the [Bisschop et al. \(2007\)](#) data shows that the NH_2CHO column densities may have larger uncertainties than quoted in their figures and tables. We have therefore re-analysed all NH_2CHO data from that paper taking larger uncertainties into account. In general, this leads to lower NH_2CHO column densities. Even using the upper limits from this re-analysis as well as those from [Isokoski et al. \(2013\)](#) (which were obtained with generous error bars), the NH_2CHO_{upper}/CH_3OH ratios are significantly lower than the models. This suggests that both the methylamine and formamide abundances are too high in the models.

The Sgr B2 detections tend to have lower CH_3NH_2/NH_2CHO and CH_3NH_2/CH_3OH ratios than our upper limits and are also somewhat below the models, but generally do not differ more than a factor of a few. The Sgr B2 NH_2CHO/CH_3OH ratios are also closer to the models results, at least for the faster models. However, the Orion Compact Ridge NH_2CHO/CH_3OH value from [Crockett et al. \(2014\)](#) is comparable to that found for our sources and clearly lower than the models. Further observations are needed to determine to what extent Sgr B2 is a special case.

To further elucidate the differences between theory and our and the Sgr B2 observations, an additional analysis was made of the CH_3NH_2/CH_3CN ratio. These results are listed in Table 4. Acetonitrile is produced in the gas-phase, but more abundantly on grains: an important route to its formation is via $CH_3^+ + CN^* \rightarrow CH_3CN$, according to [Garrod et al. \(2008\)](#). This would mean that both molecules compete for the methyl radical on the surface, thus relating the two molecules.

Our observed ratios involving CH_3CN are clearly at odds with the theoretical predictions. The observed CH_3NH_2/CH_3CN ratios are in most cases an order of magnitude lower than theory and approach the observed ratios for Sgr B2. However,

Table 4. Upper limit column densities and abundance ratios for methylamine.

Source	CH ₃ NH ₂ /CH ₃ CN	CH ₃ CN/CH ₃ OH
Model F	5.5E+01	6.3E-04
Model M	3.8E+01	2.6E-03
Model S	1.5E+01	8.6E-03
AFGL 2591	<5.3	<7.5E-02
G24.78	<5.1E-01	2.1E-01
G31.41+0.31	<3.6	5.9E-02*
G75.78	<1.9E+01	1.6E-02
IRAS 18089-1732	<8.9	1.1E-02*
IRAS 20126+4104	<4.3E+01	5.2E-02
NGC 7538 IRS1	<2.5	6.8E-02
W3(H ₂ O)	<7.2	7.0E-03
W 33A	<2.1	1.4E-01
Sgr B2 ^a	1.2	1.5E-02
Sgr B2(N) ^b	3.0E-01	1.1E-01
Sgr B2(M) ^b	2.5E-01	6.7E-02
Sgr B2(N) ^c	5.9E+01	1.7E-02
Orion Compact Ridge ^d	–	1.1E-02

Notes. Abundance ratios for methylamine. The values for CH₃OH and CH₃CN were taken from [Bisschop et al. \(2007\)](#) and [Isokoski et al. \(2013\)](#). (*) Ratio derived from optically thin ¹³C isotope.

References. ^(a) [Turner \(1991\)](#); ^(b) [Belloche et al. \(2013\)](#); ^(c) [Neill et al. \(2014\)](#); and ^(d) [Crockett et al. \(2014\)](#).

the observed CH₃CN/CH₃OH ratios are 1–2 orders of magnitude higher than theoretical predictions. Both these cases point to CH₃CN being underproduced in the models.

Finally, abundance ratios, with some notable exceptions, do not vary more than an order of magnitude between different sources, as also found by [Bisschop et al. \(2007\)](#) for other species.

5. Discussion

Despite a significant number of successfully identified molecules (see [Table A.1](#), for examples of W3(H₂O) and G31.41+0.31), only upper limits were found for methylamine in the various hot cores, limiting the conclusions that can be drawn. Nevertheless, trends are seen in our abundance ratios. The results suggest that theoretically predicted abundances for both methylamine and formamide are too high. In contrast, acetonitrile is found to be underproduced in the models. In the following, each of these species is discussed individually.

5.1. CH₃NH₂

[Garrod et al. \(2008\)](#) suggest that methylamine is primarily formed by grain-surface chemistry using UV to create the CH₃ and NH₂ radicals from photodissociation of primarily CH₄ and NH₃. Perhaps the amount of UV processing is overestimated in these models. An alternative route is hydrogen atom addition to solid HCN, proposed by [Theule et al. \(2011\)](#) and found to lead to both CH₂NH (methanimine) and CH₃NH₂. [Walsh et al. \(2014\)](#) find in their models that methylamine is indeed efficiently formed on grains at 10 K by atom addition reactions to solid CH₂NH. [Burgdorf et al. \(2010\)](#) have detected HCN ice on Triton, but so far no detection of solid HCN has been made in the interstellar medium (ISM). Methanimine is actually readily observed in the gas-phase ([Turner 1991](#); [Nummelin et al. 1998](#); [Belloche et al. 2013](#)) so the presence of both species makes

the H-atom addition scheme probable. However, [Halfen et al. \(2013\)](#) detect CH₂NH in Sgr B2(N) at a rotational temperature of 44 K, which is distinctly colder than the 159 K observed for CH₃NH₂, suggesting that the two molecules may not co-exist. An alternative route would therefore be to form these molecules by two different gas-phase reaction pathways (CH[•](g) + NH₃(g) → CH₂NH + H and CH₃[•](g) + NH₃(g) → CH₃NH₂ + H), with CH being present primarily in the colder outer envelope and CH₃ in the warmer center. Further modeling is needed to determine whether these gas-phase reactions can reproduce the observed abundances quantitatively.

5.2. NH₂CHO

Formamide also appears to be overproduced in the hot core model. Since [Garrod et al. \(2008\)](#) use both gas-phase, radical and atom addition reactions to form formamide, it is difficult to pin down where the discrepancies could come from. It is known that NH₂CHO is formed in CO:NH₃ mixtures after UV and electron irradiation ([Grim et al. 1989](#); [Demyk et al. 1998](#); [Jones et al. 2011](#)) and it has also been proposed that it can form from H- and N-atom addition to solid CO ([Tielens & Charnley 1997](#)). Gas-phase formation from CO and NH₃ is viable as well ([Hubbard et al. 1975](#)), although these experiments were conducted under high-pressure conditions, not the low pressures applicable in the ISM. Further quantification of both gas-phase and solid phase routes through laboratory experiments is needed. Recent laboratory experiments by [Fedoseev et al. \(2015\)](#) do not find NH₂CHO production in H- and N-atom bombardment studies of solid CO, consistent with a large barrier for H- addition to HNCO found in ab initio calculations ([Nguyen et al. 1996](#)), so perhaps the efficiency of this route has been overestimated in the models. An alternative solution would be that the high-mass sources studied here have not gone through a long (pre-stellar) phase in which the dust temperature was low enough for CO to be frozen out and turned into other molecules.

5.3. CH₃CN

The clear mismatches between theory and observations for the ratios involving CH₃CN point toward an underproduction of acetonitrile by more than an order of magnitude in the models. As with formamide, gas-phase, radical and atom addition reactions contribute to the formation of CH₃CN in the models, making it difficult to determine the cause. The main formation route in the models by radical addition of solid CH₃[•] and solid CN[•] has never experimentally been investigated. It would therefore be useful to determine if this is a viable solid state formation route and if it potentially has a higher efficiency than assumed.

Alternatively it is possible that photodestruction of solid acetonitrile is not as efficient as assumed in the models. [Gratier et al. \(2013\)](#) find high gas-phase CH₃CN abundances in the Horsehead PDR, indicative of a high photodesorption rate and slow destruction of CH₃CN in the ice. [Bernstein et al. \(2004\)](#) indeed find slower photolysis of solid CH₃CN compared with other organic molecules. If such a slower photodissociation rate would also hold for gas-phase CH₃CN, it would be an attractive explanation why the CH₃CN rotational temperatures are generally higher than those of other complex molecules (e.g., [Bisschop et al. \(2007\)](#) and many other hot core studies), since the molecule could then approach the protostar closer before being destroyed. However, the gas phase photoabsorption cross sections of CH₃CN are well determined and if the bulk of these

absorptions lead to dissociation this would result in a photodissociation rate of gaseous CH₃CN at least as fast as that of CH₃OH (van Dishoeck et al. 2006).

Another important parameter for all molecules studied here is the mobility of radicals and neutral molecules on the surface assumed in the gas-grain models. For many species no experimental data are available on diffusion barriers, only theoretically-inspired guesses. Observational evidence suggests that at least parts of the ice mantles are segregated in CO-rich and CO-poor layers (Tielens et al. 1991; Pontoppidan et al. 2008). Therefore, more knowledge of the structure of ice mantles and the mobility of radicals and neutral molecules as a function of surface temperature and in various chemical environments is necessary to determine if addition reactions are likely to happen and at which rates.

5.4. Prospects for ALMA

In the near future, much deeper searches for CH₃NH₂ can be carried out by ALMA (Appendix B). Figure B.1 shows that the strongest transitions within Band 6 are mainly located between 240 and 275 GHz and in Band 7 around 310, 340 and 355 GHz. In Table B.1 the strongest transitions in ALMA's Band 6 and 7 are listed. It becomes apparent that lines covered by Band 7 are more intense, but at the cost of a lower line density.

Estimates done for the W 33A source with the CASSIS line analysis software and the ALMA Sensitivity Calculator show that ALMA should be able to reach the 3 σ detection limits for the CH₃NH₂ lines around 236 GHz in less than 1 h of integration time, assuming the column density for methylamine of 1.2 \times 10¹⁴ cm⁻² as found by Turner (1991) in a large beam and two orders of magnitude lower than those inferred here for a small source size. This estimate assumes a spectral resolution of 0.64 km s⁻¹ as used in our JCMT data, the number of ALMA antennas set to 34 (as in Cycle 2) and a synthesized beam of 1.1'', appropriate for the W33A hot core (100 K radius).

6. Conclusions

We have analysed nine hot core regions in search of methylamine. The molecule has not been convincingly detected, so upper limit abundances are determined for all the sources. From these limits, ratios of methylamine to other molecules (NH₂CHO, CH₃OH, CH₃CN) have been determined and compared with theory and Sagittarius B2 surveys. Our conclusions are as follows:

1. Trends in our results indicate that both methylamine and formamide are overproduced in the models of Garrod et al. (2008). Acetonitrile is underproduced with respect to these models. This is especially true for the slow models.
2. Abundance ratios do not differ more than an order of magnitude between various sources suggesting that the (nitrogen) chemistry is very similar between hot cores, as has been found previously for other species.
3. More (laboratory) studies are needed to clarify the formation pathway of methylamine and to determine differences and similarities with formamide, methanimine and, to a lesser extent, acetonitrile formation.
4. The upper limits determined for CH₃NH₂ here can guide future more sensitive observations, especially with ALMA.

Based on the ratios found in the Sgr B2 observations it is very likely that ALMA will reach the detection limit for methylamine in the sources studied here. Particularly strong transitions and spectral regions to target with ALMA are given.

Acknowledgements. We would like to thank C. Walsh, I. San Jose García, M. Drozdovskaya, N. van der Marel, M. Kama, M. Persson, J. Mottram, G. Fedoseev, M. H. D. van der Wiel and H. Linnartz for their support and input on this project. Thoughtful comments by the referee are much appreciated. Astrochemistry in Leiden is supported by the Netherlands Research School for Astronomy (NOVA), by a Royal Netherlands Academy of Arts and Sciences (KNAW) professor prize, and by the European Union A-ERC grant 291141 CHEMPLAN.

References

- Belloche, A., Müller, H. S. P., Menten, K. M., Schilke, P., & Comito, C. 2013, *A&A*, **559**, A47
- Bernstein, M. P., Ashbourn, S. F. M., Sandford, S. A., & Allamandola, L. J. 2004, *ApJ*, **601**, 365
- Bisschop, S. E., Jørgensen, J. K., van Dishoeck, E. F., & de Wachter, E. B. M. 2007, *A&A*, **465**, 913
- Blake, G. A., Sutton, E. C., Masson, C. R., & Phillips, T. G. 1987, *ApJ*, **315**, 621
- Burgdorf, M., Cruikshank, D. P., Dalle Ore, C. M., et al. 2010, *ApJ*, **718**, L53
- Caselli, P., & Ceccarelli, C. 2012, *A&ARv.*, **20**, 56
- Crockett, N. R., Bergin, E. A., Neill, J. L., et al. 2014, *ApJ*, **787**, 112
- Demyk, K., Dartois, E., D'Hendecourt, L., et al. 1998, *A&A*, **339**, 553
- Ehrenfreund, P., & Charnley, S. B. 2000, *ARA&A*, **38**, 427
- Fedoseev, G., Ioppolo, S., Zhao, D., Lamberts, T., & Linnartz, H. 2015, *MNRAS*, **446**, 439
- Fontani, F., Pascucci, I., Caselli, P., et al. 2007, *A&A*, **470**, 639
- Fourikis, N., Takagi, K., & Morimoto, M. 1974, *ApJ*, **191**, L139
- Garrod, R. T., & Herbst, E. 2006, *A&A*, **457**, 927
- Garrod, R. T., Weaver, S. L. W., & Herbst, E. 2008, *ApJ*, **682**, 283
- Gibb, E. L., Whittet, D. C. B., Schutte, W. A., et al. 2000, *ApJ*, **536**, 347
- Gratier, P., Pety, J., Guzmán, V., et al. 2013, *A&A*, **557**, A101
- Grim, R., Schutte, W., Schmitt, B., & Greenberg, M. 1989, in *Interstellar Dust*, eds. L. J. Allamandola, & A. G. G. M. Tielens, IAU Symp., **135**, 245
- Halfen, D. T., Ilyushin, V., & Ziurys, L. M. 2011, *ApJ*, **743**, 60
- Halfen, D. T., Ilyushin, V. V., & Ziurys, L. M. 2013, *ApJ*, **767**, 66
- Herbst, E., & van Dishoeck, E. F. 2009, *ARA&A*, **47**, 427
- Hubbard, J., Voecks, G., Hobby, G., et al. 1975, *J. Mol. Evol.*, **5**, 223
- Isokoski, K., Bottinelli, S., & van Dishoeck, E. F. 2013, *A&A*, **554**, A100
- Jones, B. M., Bennett, C. J., & Kaiser, R. I. 2011, *ApJ*, **734**, 78
- Kaifu, N., Morimoto, M., Nagane, K., et al. 1974, *ApJ*, **191**, L135
- Maret, S., Hily-Blant, P., Pety, J., Bardeau, S., & Reynier, E. 2011, *A&A*, **526**, A47
- Neill, J. L., Bergin, E. A., Lis, D. C., et al. 2014, *ApJ*, **789**, 8
- Nguyen, M. T., Sengupta, D., Vereecken, L., Peeters, J., & Vanquickenborne, L. G. 1996, *J. Phys. Chem.*, **100**, 1615
- Nummelin, A., Bergman, P., Hjalmarsen, Å., et al. 1998, *ApJS*, **117**, 427
- Nummelin, A., Bergman, P., Hjalmarsen, Å., et al. 2000, *ApJS*, **128**, 213
- Öberg, K. I. 2009, Ph.D. Thesis, Leiden Observatory, Leiden University, Leiden, The Netherlands
- Pickett, H. M., Poynter, R. L., Cohen, E. A., et al. 1998, *J. Quant. Spectr. Rad. Transf.*, **60**, 883
- Pontoppidan, K. M., Boogert, A. C. A., Fraser, H. J., et al. 2008, *ApJ*, **678**, 1005
- Rathborne, J. M., Jackson, J. M., Zhang, Q., & Simon, R. 2008, *ApJ*, **689**, 1141
- Schilke, P., Groesbeck, T. D., Blake, G. A., & Phillips, T. G. 1997, *ApJS*, **108**, 301
- Sutton, E. C., Peng, R., Danchi, W. C., et al. 1995, *ApJS*, **97**, 455
- Theule, P., Borget, F., Mispelaer, F., et al. 2011, *A&A*, **534**, A64
- Tielens, A. G. G. M., & Charnley, S. B. 1997, *Origins of Life and Evolution of the Biosphere*, **27**, 23
- Tielens, A. G. G. M., Tokunaga, A. T., Geballe, T. R., & Baas, F. 1991, *ApJ*, **381**, 181
- Turner, B. E. 1991, *ApJS*, **76**, 617
- van Dishoeck, E. F., & Blake, G. A. 1998, *ARA&A*, **36**, 317
- van Dishoeck, E. F., Jonkheid, B., & van Hemert, M. C. 2006, *Faraday Discussions*, **133**, 231
- Walmsley, C. M. 1992, in *Chemistry and Spectroscopy of Interstellar Molecules*, ed. D. K. Bohme, 267
- Walsh, C., Millar, T. J., Nomura, H., et al. 2014, *A&A*, **563**, A33

Appendix A: Methylamine and other transitions

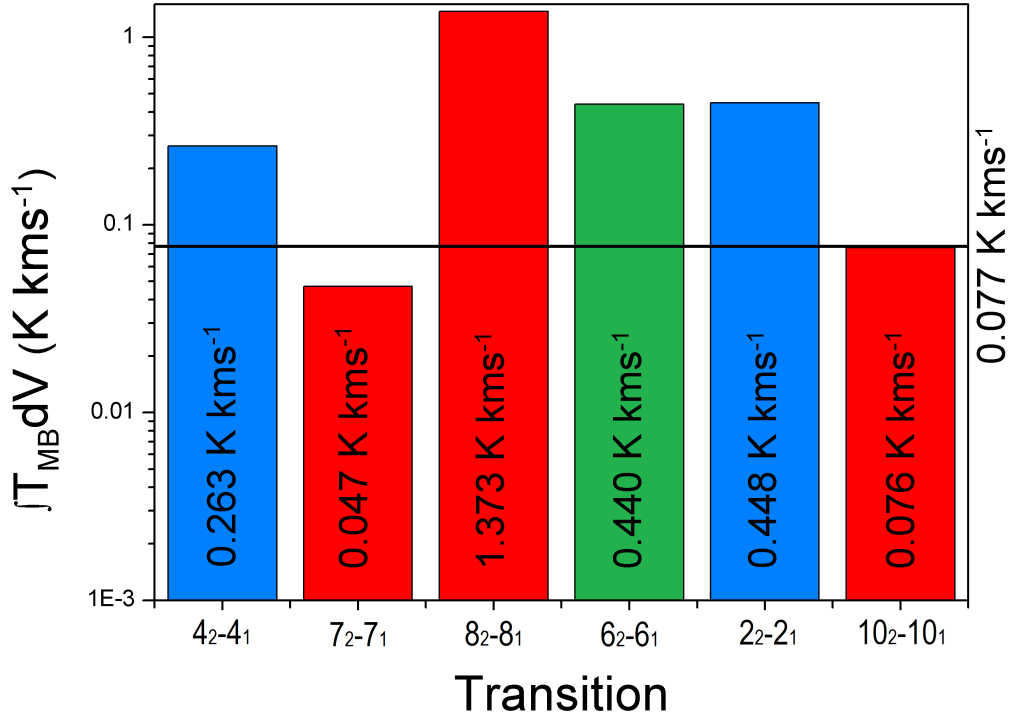


Fig. A.1. Bargraph plot of the integrated main-beam intensities for the six investigated methylamine transitions. $\int T_{\text{MB}} dV$ values were calculated for a total column density of $3.4 \times 10^{17} \text{ cm}^{-2}$ as inferred toward G31.41+0.31 from the $6_2 \rightarrow 6_1$ transition, assuming a rotational temperature of 120 K. The horizontal line shows the $0.077 \text{ K km s}^{-1}$ 3σ value for G31.41+0.31. It is unlikely that the detection of the 236 408 feature (green) in this hot core is methylamine, since the main-beam intensities of other CH_3NH_2 transitions are above the 3σ value. Particularly the $4_2 \rightarrow 4_1$ and $2_2 \rightarrow 2_1$ transition (blue) should be visible in our spectra. The remaining transitions (red) are either below detection limit or not observed toward this source.

Table A.1. All identified transitions for the sources G31.41+0.31 and W3(H₂O), with integrated peak area listed.

Species	Freq. (MHz)	E_{up} (K)	A (s ⁻¹)	Transition	G31.41+0.31 (K km s ⁻¹)	W3(H ₂ O) (K km s ⁻¹)
CH ₃ OCHO	228 628.876	118.8	1.66E-04	18 ₅₁₃₂ → 17 ₅₁₂₂	–	0.39
CH ₃ OCHO	228 651.404	118.8	1.66E-04	18 ₅₁₃₀ → 17 ₅₁₂₀	–	0.53
CH ₃ COCH ₃	228 668.358	85.4	1.69E-04	14 ₉₆₁ → 13 ₈₅₂	–	0.24
CH ₃ OCHO	229 388.947	217.0	1.62E-05	23 ₉₁₅₀ → 23 ₈₁₆₀	0.79	–
CH ₃ OCHO	229 405.021	110.7	1.75E-04	18 ₃₁₅₂ → 17 ₃₁₄₂	2.18	0.78
CH ₃ OCHO	229 420.342	110.7	1.75E-04	18 ₃₁₅₀ → 23 ₃₁₄₀	1.86	0.71
CH ₃ OCHO	229 504.724	134.3	1.18E-05	20 ₃₁₇₀ → 19 ₄₁₆₀	1.52	–
CH ₃ OH	229 589.056	374.4	2.08E-05	15 ₄₀ → 16 ₃₀	2.58	1.06
CH ₃ OH	229 758.756	89.1	4.19E-05	8 ₁₀ → 7 ₀₀	7.17	–
CH ₃ OCHO	236 355.948	128.0	1.93E-04	20 ₃₁₈₁ → 19 ₃₁₇₁	2.38	–
CH ₃ OCHO	236 365.574	128.0	1.93E-04	20 ₃₁₈₀ → 19 ₃₁₇₀	1.93	–
CH ₃ NH ₂	236 408.788	60.8	5.94E-05	6 ₂₁ → 6 ₁₀	0.44	–
HCCCN	236 512.777	153.2	1.05E-03	26 → 25	4.67	2.27
H ₂ CS	236 726.770	58.6	1.91E-04	7 ₁₇ → 6 ₁₆	7.54	5.75
CH ₃ OCHO	236 743.697	129.6	1.86E-04	19 ₅₁₅₁ → 18 ₅₁₄₁	2.21	? ^a
CH ₃ OCHO	236 759.687	129.6	1.86E-04	19 ₅₁₅₀ → 18 ₅₁₄₀	1.40	0.53
CH ₃ OCHO	236 800.589	136.7	1.80E-04	19 ₆₁₄₁ → 18 ₆₁₃₁	1.21	?
CH ₃ OCHO	236 810.314	136.7	1.81E-04	19 ₆₁₄₀ → 18 ₆₁₃₀	2.50	1.20
CH ₃ OH	236 936.089	260.2	2.79E-05	14 ₁₀ → 13 ₂₀	2.74	1.91
CH ₃ OCHO	236 975.844	320.3	2.01E-04	22 ₁₂₂₄ → 21 ₁₂₁₄	0.86	0.33
CH ₃ OCHO	236 976.390	320.3	2.01E-04	22 ₀₂₂₅ → 21 ₀₂₁₀	0.86	0.33
CH ₃ OCHO	236 975.844	320.3	2.01E-04	22 ₁₂₂₄ → 21 ₁₂₁₄	1.19	0.52
CH ₃ OCHO	236 976.390	320.3	2.01E-04	22 ₀₂₂₅ → 21 ₀₂₁₅	1.19	0.52
CH ₃ OCH ₃	237 046.092	31.3	2.33E-05	7 ₂₅₃ → 6 ₁₆₃	2.90	0.80
CH ₃ OCH ₃	237 046.106	31.3	2.33E-05	7 ₂₅₂ → 6 ₁₆₂	2.90	0.80
CH ₃ OCH ₃	237 048.797	31.3	2.32E-05	7 ₂₅₁ → 6 ₁₆₁	2.90	0.80
CH ₃ OCH ₃	237 051.495	31.3	2.33E-05	7 ₂₅₀ → 6 ₁₆₀	2.90	0.80
SO ₂	237 068.870	94.0	1.14E-04	12 ₃₉ → 12 ₂₁₀	1.07	1.96
OC ³⁴ S	237 273.635	119.6	3.88E-05	20 → 19	1.24	0.58
CH ₃ OCHO	237 297.482	128.0	1.95E-04	20 ₂₁₈₂ → 19 ₂₁₇₂	?	2.45
CH ₃ OCHO	237 309.540	131.6	1.98E-04	21 ₂₂₀₁ → 20 ₂₁₉₁	?	2.45
CH ₃ OCHO	237 315.082	131.6	1.98E-04	21 ₂₂₀₀ → 20 ₂₁₉₀	?	2.45
CH ₃ OCHO	237 344.870	131.6	1.98E-04	21 ₁₂₀₂ → 20 ₁₁₉₂	3.48	1.19
CH ₃ OCHO	237 350.386	131.6	1.98E-04	21 ₁₂₀₀ → 20 ₁₁₉₀	3.48	1.19
OCS	243 218.040	122.6	4.18E-05	20 → 19	–	2.95
CH ₃ OCH ₃	259 982.561	226.6	7.27E-05	20 ₅₁₆₂ → 20 ₄₁₇₂	–	1.54
CH ₃ OCH ₃	259 982.596	226.6	7.27E-05	20 ₅₁₆₃ → 20 ₄₁₇₃	–	1.54
CH ₃ OCH ₃	259 984.480	226.6	7.27E-05	20 ₅₁₆₁ → 20 ₄₁₇₁	–	1.54
CH ₃ OCH ₃	259 982.561	226.6	7.27E-05	20 ₅₁₆₀ → 20 ₄₁₇₀	–	1.54
NH ₂ CHO	260 189.848	92.4	1.25E-03	12 ₂₁₀ → 11 ₂₉	–	1.46
H ¹³ CO+	260 255.339	25.0	1.33E-03	3 → 2	–	11.76
CH ₃ OCH ₃	260 327.165	208.3	7.21E-05	19 ₅₁₅₂ → 19 ₄₁₆₂	–	1.27
CH ₃ OCH ₃	260 327.238	208.3	7.21E-05	19 ₅₁₅₃ → 19 ₄₁₆₃	–	1.27
CH ₃ OCH ₃	260 329.312	208.3	7.21E-05	19 ₅₁₅₁ → 19 ₄₁₆₁	–	1.27
CH ₃ OCH ₃	260 331.422	208.3	7.21E-05	19 ₅₁₅₀ → 19 ₄₁₆₀	–	1.27
SiO	260 518.020	43.8	7.21E-05	6 → 5	–	9.24

Notes. ^(a) Identified transition where it was not possible to determine the peak area.

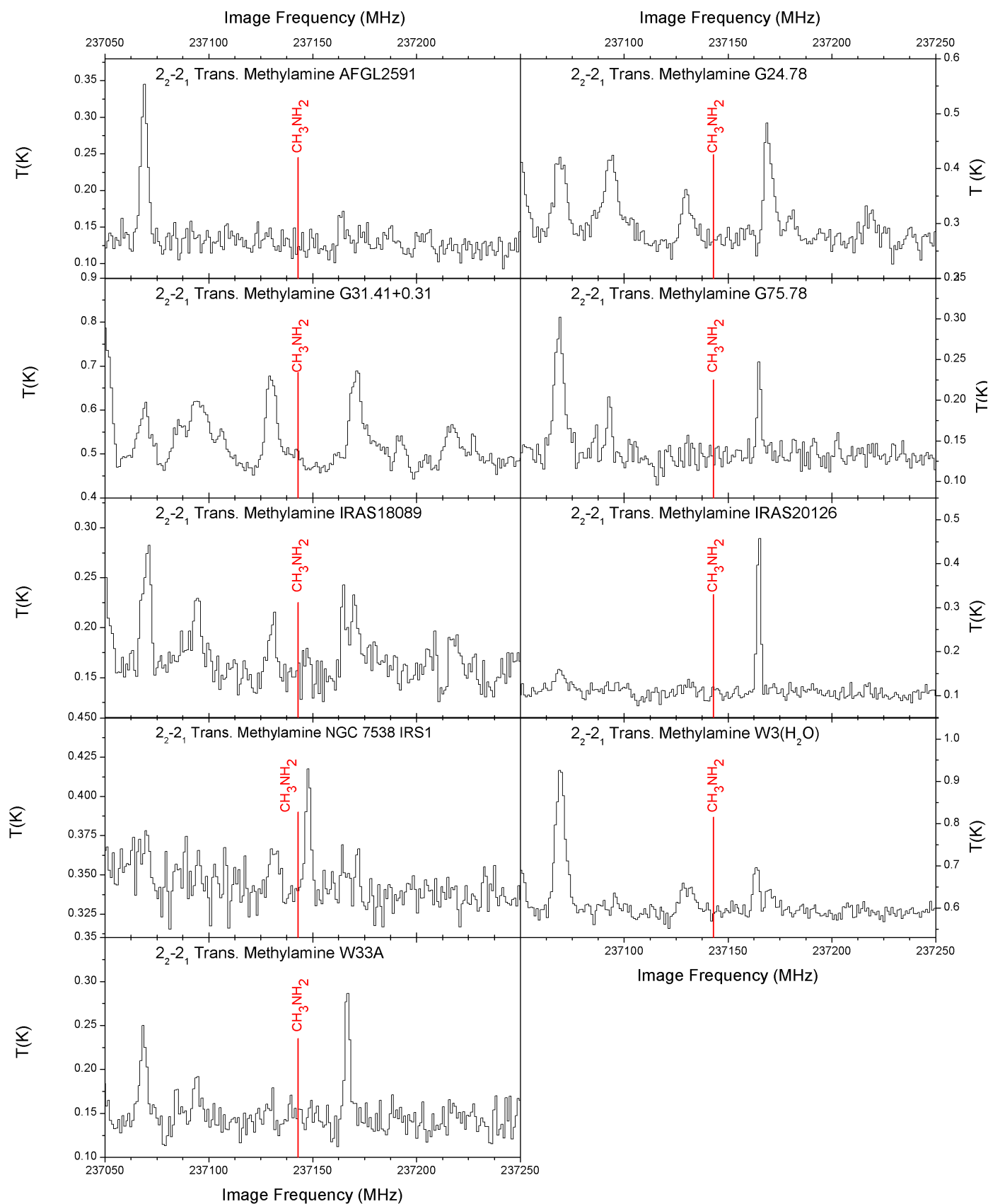


Fig. A.2. Blow-up of the spectral region around the $2_2 \rightarrow 2_1$ transition at 237143 MHz of all analysed hot cores. Despite being a particularly strong transition, it was not observed in any of the spectra.

Appendix B: ALMA

In the following figure the simulated spectrum of methylamine is shown for a column density of $1.0 \times 10^{15} \text{ cm}^{-2}$ at an excitation temperature of 120 K. Simulations were done with CASSIS using the JPL spectroscopic database. The frequency ranges were taken to cover ALMA Bands 6 and 7. The resolution was set at 0.1 MHz for this spectrum.

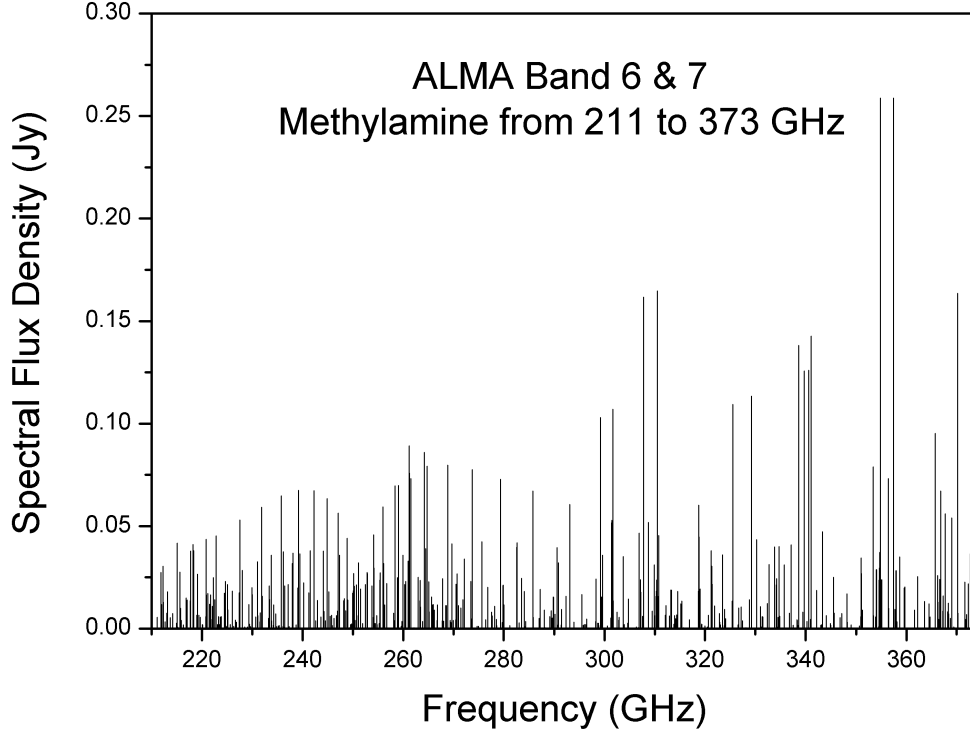


Fig. B.1. 211 to 373 GHz spectrum of methylamine, covering ALMA bands 6 and 7. A column density of 10^{15} cm^{-2} , T_{rot} and beam size of $1''$ are used.

Table B.1. Methylamine transition target candidates for ALMA Band 6 and 7.

Transition	Freq. (MHz)	E_{up} (K)	A (s^{-1})
$7_{2,6} \rightarrow 7_{1,6}$	227 498.06	75.4	4.80E-05
$5_{2,6} \rightarrow 5_{1,6}$	232 003.95	47.7	4.73E-05
$8_{2,3} \rightarrow 8_{1,2}$	235 735.04	92.8	6.13E-05
$7_{2,2} \rightarrow 7_{1,3}$	239 209.63	75.8	6.29E-05
$6_{2,3} \rightarrow 6_{1,2}$	242 262.02	60.9	6.39E-05
$5_{2,2} \rightarrow 5_{1,3}$	244 886.90	48.1	6.42E-05
$8_{0,5} \rightarrow 7_{1,5}$	259 042.46	77.0	5.73E-05
$6_{2,2} \rightarrow 6_{1,3}$	261 252.89	60.9	7.14E-05
$8_{0,2} \rightarrow 7_{1,3}$	261 563.15	76.8	5.98E-05
$4_{1,5} \rightarrow 3_{0,5}$	264 172.21	25.9	8.74E-05
$8_{2,2} \rightarrow 8_{1,3}$	268 898.14	92.8	7.44E-05
$9_{0,5} \rightarrow 8_{1,5}$	299 189.80	96.1	8.78E-05
$9_{0,3} \rightarrow 8_{1,2}$	301 654.091	95.9	9.11E-05
$5_{-1,3} \rightarrow 4_{0,2}$	307 791.75	36.3	1.44E-04
$14_{2,2} \rightarrow 14_{-1,3}$	310 750.84	240.0	8.33E-05
$10_{0,5} \rightarrow 9_{1,5}$	338 628.32	117.3	1.25E-04
$10_{0,2} \rightarrow 9_{-1,3}$	341 059.48	117.1	1.30E-04
$6_{1,2} \rightarrow 5_{0,3}$	354 843.73	49.2	2.16E-04
$6_{1,5} \rightarrow 5_{0,5}$	357 440.12	49.5	2.16E-04
$3_{2,4} \rightarrow 2_{1,4}$	370 166.34	28.4	2.11E-04